Proceedings of the 2021 Design of Medical Devices Conference
DMD2021
April 12-15, 2021, Minneapolis, MN, USA

DMD2021-1037

DESIGN OF A FLEXURE-BASED COMPLIANT GRASPER FOR THE MASTER ARM OF A SURGICAL ROBOT

Karthik Chandrasekaran
Robotics lab,
Department of Engineering Design,
Indian Institute of Technology Madras,
India

Adarsh Somayaji
Robotics lab,
Department of Engineering Design,
Indian Institute of Technology Madras,
India

Asokan Thondiyath
Robotics lab,
Department of Engineering Design,
Indian Institute of Technology Madras,
India

ABSTRACT

A master arm of a tele-operated surgical robot serves as an input device to the system. A master arm typically has 6 Degrees of Freedom (DoF) input apart from grasping input used to control the grasping motion of the surgical tool located at the slave arm. The typical design of a master arm grasper makes use of either a gear driven or a crank-slider linkage to capture the grasping input from the surgeon. Such a mechanism has several moving components and needs joints with minimal clearance for reliable operation. A compliant mechanism that features a joint-less design offers superior performance and would serve as an ideal replacement for such a mechanism. This paper presents the design and analysis of a master arm grasper based on a partially compliant mechanism. An inherent advantage of the proposed mechanism for this application is the reduced number of components. Design details and the pseudo-rigid body analysis of the grasper are presented. A prototype of the grasper has been fabricated, and experimental verifications were carried out. The grasper was integrated into a custom-built master arm manipulator to demonstrate its utility in a surgical robot. Results show that the compliant grasper performs well for its intended purpose.

Keywords: robotic surgery, master arm grasper, compliant mechanisms, flexures, pseudo rigid body model

NOMENCLATURE

DoF	Degree of Freedom
PRBM	Pseudo-Rigid Body Model
E	Modulus of elasticity of the print resin
F	applied grasper force
I	area moment of inertia of small length flexure
L	equivalent length at which force F is applied
R	reaction force offered by spring in potentiometer
a	distance from center of circular profile to characteristic pivot
b	depth of small length flexure
h	thickness of small length flexure
l	length of small length flexure
m	vertical distance of characteristic pivot from origin O
n	distance from face of follower to its imaginary apex
r	radius of circular profile of grasper
s	horizontal distance from follower face to origin O
(p,q)	coordinates of center of circular profile of grasper
F_f	force required to bend small length flexure by angle $\delta\theta$ with follower removed
F_2	active force required to balance force R
x_1	distance from imaginary apex of follower to origin O
x_d	spring deflection
θ	grasper input angle
β	angle between line of action of force F_2 and x-axis
γ	half wedge angle of follower
$\emptyset_s$	friction angle
μ_s	static coefficient of friction
σ_{max}	maximum bending stress of small length flexure

1. INTRODUCTION

Robot-assisted laparoscopic surgery has gained considerable popularity in the last two decades. Currently available robotic surgical systems are tele-manipulated, in which the command from a master input device is used to control a slave arm remotely [1]. A typical slave arm has 7 Degrees of Freedom (DoF), with 6 DoF for the surgical tool and the arm, and the other DoF being the tool gripper motion [2]. The master arm has a grasper for the surgeon to hold and provide the grip command to the surgical tool gripper. The role of master arm grasper is to measure the opening angle command given by a surgeon and relay it to the surgical tool of the slave manipulator. The design of the master arm grasper is critical, given the ease of use and the surgeon's comfort. Traditional, off the shelf master

arms like Phantom® Premium™ [3] allow the only measurement of open/close command with a push button. The commercially available da Vinci® surgical system uses a four-bar crank-slider mechanism for its master arm grasper. The crank of the four-bar mechanism serves as the grasper, and the slider is connected to a linear position sensing element. This mechanism enables the measurement of the opening angle of the grasper. Two such four bars are connected symmetrically [4]. Such a grasper is infinitely rotatable about its longitudinal axis and is removable, enabling it to be modular. Grasper design of dV-Trainer® from mimic technologies [5] has two spring-loaded jaws with intermeshing gears that allow them to move symmetrically about a rotational axis. Similar to daVinci® surgical system, this system also enables measuring the precise opening angle of the master arm grasper. Such a complex set of linkages can be replaced with a monolithic compliant mechanism, which also offers an avenue for weight reduction. Most of the commercially available robots and robotic trainers use a precision grip [4-6] over other types of grips for good control over the grasp DoF of the surgical grasper.

Kota, S. et al. [7] and Thomas T. L. et al. [8] have shown that for surgical applications, compliant mechanisms offer vital advantages such as joint-free design, the absence of wear and debris, and lubrication-free operation. Also, the need for a separate return spring required to restore the grasper to its neutral position when the pinching force is removed is eliminated. In this paper, the design of a partially compliant grasper for the master arm of a surgical robot or a tele-surgical trainer is presented. The paper is organized as follows; Section 2.1 describes the design of the proposed device and its pseudo-rigid body analysis. Further sections elaborate on the flexure stress analysis, grasper pinching force analysis, prototyping and testing of the proposed device. Finally, the semi-compliant grasper is integrated into a custom-built master arm assembly to demonstrate its utilization in a tele-operated robotic setup.

2. MATERIALS AND METHODS

2.1 Compliant grasper design

The mechanical advantage of a fully compliant statically unbalanced mechanism is some fraction of the mechanical advantage of an equivalent rigid body mechanism [9]. Since fully compliant mechanisms need larger energy for actuation, a semi-compliant mechanism is chosen for the master arm grasper design. A statically unbalanced compliant mechanism can return to its neutral position on its own. Hence, we have taken an approach to design a master arm grasper that is semi-compliant and satisfy the design requirements without the need for static balancing. The proposed design for the grasper consists of two components, a monolithic pair of grasper and a follower. A Computer Aided Design (CAD) of the grasper is shown in Figure 1. A small length flexural pivot [10], as shown in Figure 1, provides compliance for the grasper. The inner portion of each grasper has a circular profile. There is a wedge-shaped follower with a half wedge angle γ between the grasper. The follower converts the rotary motion of the grasper to linear motion, as shown in Figure 2.

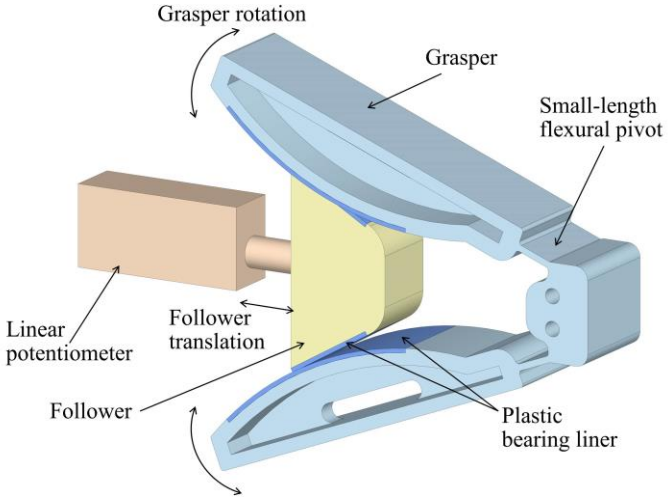

FIGURE 1: COMPUTER AIDED DESIGN OF THE COMPLIANT GRASPER ASSEMBLY

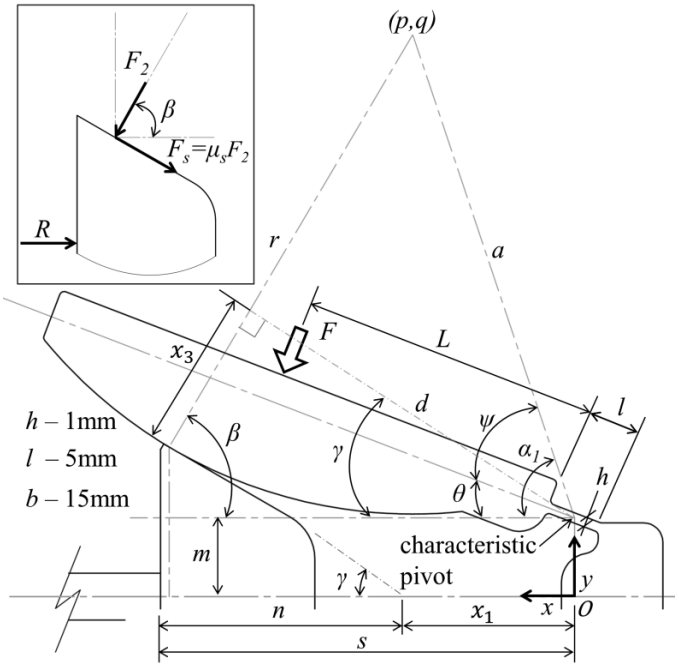

FIGURE 2: PARTIAL SKETCH OF COMPLIANT GRASPER ASSEMBLY SHOWING EQUIVALENT FORCE AND PSEUDO-RIGID BODY ANALYSIS. INSET FIGURE SHOWS A FREE BODY DIAGRAM OF THE FOLLOWER

The relation between the friction angle $\emptyset_s$ and half wedge angle γ of the follower, from [11] is given by (1).

$$\tan(\emptyset_s) = \mu_s \quad (1)$$

As the contact between the grasper and the follower is line contact, they form a higher-order pair. There is sliding friction between the joints. The static coefficient of friction μ_s of VeroClear™ photopolymer (prototype material) [12] with itself was experimentally determined to be 0.34. Since the use of any lubrication between the contact surfaces might produce objectionable debris in a surgical environment, a plastic bearing liner [13] was used to reduce the contact friction. The bearing liner

has a low friction coefficient and has good wear resistance. The coefficient of friction of the plastic bearing was experimentally determined to be 0.2 with itself. The half wedge angle γ is taken as 30 degree, which is well above the friction angle $\emptyset_s$ (11.3 degree for μ_s of 0.2) to prevent self-locking of the grasper. The bearing material is used as a lining for both the grasper and the follower as shown in Figure 1 and attached to the grasper and follower surface using the self-adhesive back of the liner. The follower is connected to a linear potentiometer (BI Technologies, Model 404) with an integrated spring. The stiffness of the spring was experimentally found out to be 0.142 N/mm. Thus, the rotary motion of the grasper can be captured by the linear motion of the potentiometer connected to the follower. The spring load of the potentiometer on the follower keeps the follower in contact with the circular profile of the grasper for all positions and prevents any backlash.

2.2 Compliant grasper design

The length of the flexural pivot is significantly smaller than the length of the grasper, and hence, a Pseudo-rigid body model (PRBM) [14] is used for analysis of the small length flexural pivot. Using PRBM, the small flexure can be modeled as two rigid links connected by a revolute joint with a torsional spring at the joint representing the revolute stiffness of the flexure. This joint is often referred to as characteristic pivot [10]. The surgeon's fingers apply a non-uniformly distributed load on the grasper. An equivalent force, *F*, at a distance *L+0.5l* from the characteristic pivot is considered for analysis, as shown in Figure 2. The length, depth and thickness of the small length flexural pivot are *l, b,* and *h,* respectively. The force *F* is a follower force and follows the rotation of the grasper. The radius of the circular profile is *r*, and its center is located at *(p, q)* from the origin, as shown in Figure 2. The angle β is constant throughout the range of motion of the grasper. Referring to Figure 2, the relation between the input angle θ and the linear position *s* of the follower can be derived as follows:

The equation of the circular profile is given by

$$(x-p)^2 + (y-q)^2 = r^2 \tag{2}$$

$$\text{where } p = a\,cos(\alpha_1) \tag{3}$$

$$q = a\,sin(\alpha_1) + m \tag{4}$$

$$\alpha_1 = \theta + \psi \tag{5}$$

$$\psi = 50° \tag{6}$$

The conical faces of the follower are tangent to the circular profile of the grasper for the entire range of motion. The conical face can be considered as a line in two dimensions which makes an angle γ with the *x*-axis. Using a point-slope form, the equation of this line is given by

$$y = (x - x_1)\,tan(\gamma) \tag{7}$$

Substituting (7) in (2), we get a quadratic equation. Since the line is tangent to the circular profile, the discriminant of this equation should be zero. The discriminant yields two roots since two lines (one below and another above the circle) can be tangent to the radius of the circular profile. Taking the root corresponding to the tangent line below the circle and solving for x_1 we get

$$x_1 = \frac{(r - m\,cos(\gamma) + a\,sin(\gamma - (\psi + \theta)))}{sin(\gamma)} \tag{8}$$

$$s = x_1 + n \tag{9}$$

$$\text{where } n = 27.7\ mm$$

$$x_3 = \sin(\gamma)(x_1 - 4.7) + x_2 \tag{10}$$

$$\text{where } x_2 = 9.4\ mm$$

A plot of the linear displacement of the follower Vs. the input angle of the grasper is shown in Figure 3. It can be seen from Figure 3, the relationship between the grasper input angle θ and the linear displacement of the follower is linear within the operating range of the grasper, even though the relationship is nonlinear. The range of operation of the grasper is taken as 4.5 degree.

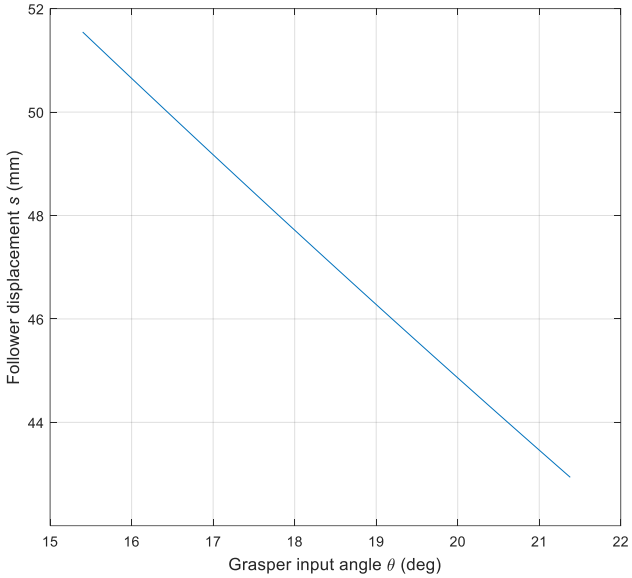

FIGURE 3: FOLLOWER LINEAR DISPLACEMENT VS GRASPER INPUT ANGLE

2.3 Flexure stress analysis

A large deflection stress analysis was performed to estimate the peak bending stresses on the flexure caused by the deflection of the grasper. The flexure was assumed to be predominantly in a state of pure bending, and only stresses caused by bending are considered for analysis. The material properties of the 3D print resin are assumed to be isotropic, and the elastic modulus E of the print resin was taken as 2 GPa [12]. The force required to deflect the grasper [10] by an angle $\delta\theta$ without the follower is given by (11).

$$F_f = \frac{K\delta\theta}{\left(L + \frac{l}{2}\right)} \tag{11}$$

$$\text{where } K = \frac{EI}{l} \tag{12}$$

The maximum bending stress is given by

$$\sigma_{max} = \frac{F_f AC}{I} \tag{13}$$

$$\text{where } A = \frac{l}{2} + \left(L + \frac{l}{2}\right) cos(\theta) \tag{14}$$

$$C = \frac{h}{2} \tag{15}$$

$$I = \frac{bh^3}{12} \tag{16}$$

The maximum bending stress σ_{max} for a deflection ($\delta\theta = 4.5$ degree) of grasper from its initial position was found to be 16 Mpa. This value is far below the flexural strength (75 Mpa) of Vero Clear [12] photo resin. A large deflection Finite Element Analysis (FEA), shown in Figure 4, was also carried out to estimate the bending stress. The FEA simulation result provides a better estimate of the stresses in the flexure as it accounts for the additional longitudinal load on the flexure. The maximum stress was found to occur at the outermost fiber of the flexure.

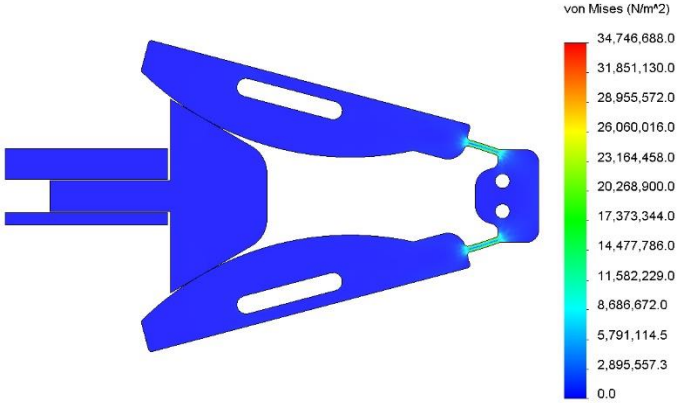

FIGURE 4: FINITE ELEMENT ANALYSIS OF GRASPER

2.4 Grasper pinching force analysis

A pinching force analysis is carried out to establish the relationship between the applied grasper force F and the displacement of the follower connected to the linear potentiometer. Referring to the inset figure in Figure 2, when the system is in a static equilibrium state, the applied force F balances the reaction force R offered by the spring in the potentiometer and the joint torque provided by the small length flexure. The equation for the reaction force of the spring R of the potentiometer was experimentally determined by applying known loads and measuring the deflection of the potentiometer. Considering force balance for the follower about the x-axis, we have

$$2F_2 \cos(\beta) = R + 2\mu_s F_2 \cos(\gamma) \tag{17}$$

$$R = 0.142x_d + 0.636 \tag{18}$$

Solving for F_2 from (17), we get

$$F_2 = \frac{0.636 + 0.142x_d}{2\cos(\beta) - 2\mu_s \cos(\gamma)} \tag{19}$$

where x_d is the deflection of the spring.

A part of the applied force F is used to counter the flexure's bending stiffness, and this force would be absent if a conventional revolute joint were used. We consider a torsional spring at the characteristic pivot to represent the revolute stiffness offered by the flexure. Force F_f can be viewed as part of the applied force F required to produce a torque at the characteristic pivot that balances the joint torque offered by the flexure given by (11). The total force F required to deflect the grasper through an angle $\delta\theta$ can be calculated by taking moment balance about the characteristic pivot shown in Figure 2.

The total applied force is given by

$$F = \frac{F_2 d + F_2 \mu_s x_3 + K\delta\theta}{\left(L + \frac{l}{2}\right)} \tag{20}$$

$$\text{where, } d = a\cos(\psi + \theta - \gamma) \tag{21}$$

2.5 Grasper prototype

The grasper and follower were made by rapid prototyping on an Objet™ polyjet printer. The material used for printing is a photo-curable VeroClear™ photopolymer [12]. Figure 5 (a) shows a prototype of the proposed compliant grasper. As discussed earlier, the contact surfaces are provided with plastic bearing liner (light blue color) to reduce sliding friction.

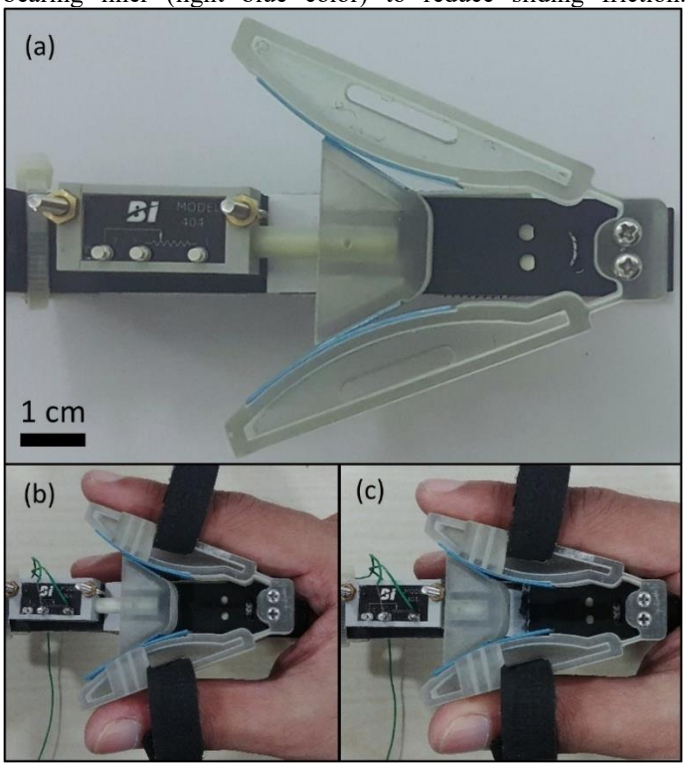

FIGURE 5: PROTOTYPE OF THE PROPOSED GRASPER ASSEMBLY

The wear of this Iglidur® tape is several orders of magnitude smaller than PTFE [13]. The follower is connected to a linear potentiometer for sensing the position. The potentiometer is calibrated to represent the change in resistance as a function of the linear position of the follower. Since an analogue potentiometer is used to measure the angular orientation of the grasper, the resolution achievable is limited only by the resolution of the analogue to digital converter. Each grasper is provided a Velcro® strap for slip-free holding by the thumb and index finger. The grasper assembly is designed with minimal mass by removing material from the least stressed portions of both grasper and follower. Figure 5 (b), (c) show the grasper in an open (neutral) and a fully closed position, respectively. The flexure recoils back to its neutral position when released because of stored strain energy and thus negates the need for a separate spring for restoring the grasper to its initial position. The spring-loaded follower maintains contact with the circular portion of the grasper and also aides the grasper to return to their neutral position quickly.

2.6 Grasper testing

A bench-test is carried out with the prototype with a separate test setup to assess the angular position of the grasper Vs. the applied grasper pinching force, as shown in Figure 6 (a). Figure 6 (b) shows a magnified view of the grasper assembly. An identical model of the proposed compliant grasper assembly is built with a provision to add tethers. The tethers enable the application of pinching force on the grasper. The whole grasper assembly was firmly bolted to a base, and a transparent acrylic sheet was provided over the grasper assembly to support two stationary diverter pulleys. These pulleys have low friction rollers that route the tethers fastened to the grasper to a force gauge mounted on a linear guide. The pulleys are located such that the force exerted on the grasper by the tethers is always normal to the grasper surface within the range of motion (4.5 deg). This is important as the force exerted should be a follower force.

The linear guide can be moved with a self-locking screw. When the force gauge is moved away from the setup, it exerts a tensile load on the pair of tethers connected to it. This tensile force, in turn, appears as the compressive force on both the grasper and exerts a pinching force on the grasper. A calibrated camera was placed above the setup to obtain the angular deflection of the grasper. Initial tests were carried out without the follower to determine the force required to actuate the grasper alone F_f.

A force of 0.6 N was required for an angle of rotation of 4.5 degree. Further tests on the grasper pinching force were carried out by application of force at a distance of 38.5 mm ($L + 0.5l$) from the characteristic pivot. A total of 10 trials were conducted with the prototype, and the mean values with standard deviation are shown in Figure 7. The theoretical estimate of the actuation force of the grasper predicted by (20) is superimposed over the experimental readings. The trend in the grasper input angle Vs. the grasper pinching force has a reasonable agreement with the theoretical estimate.

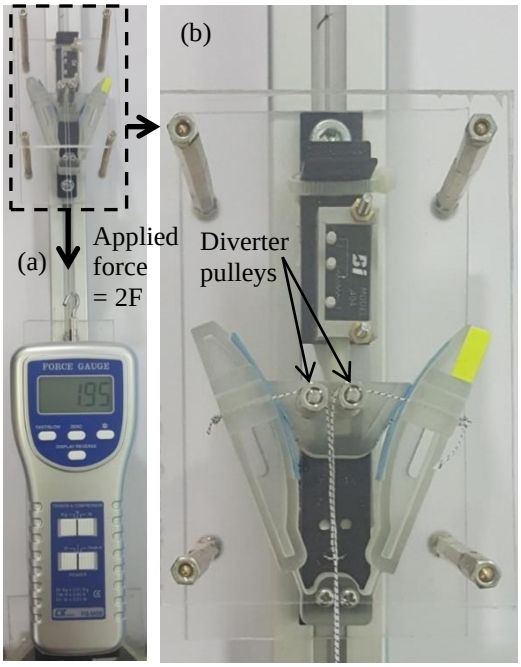

FIGURE 6: (a) EXPERIMENTAL TEST SETUP FOR GRASPER TESTING (b) MAGNIFIED VIEW OF GRASPER ASSEMBLY

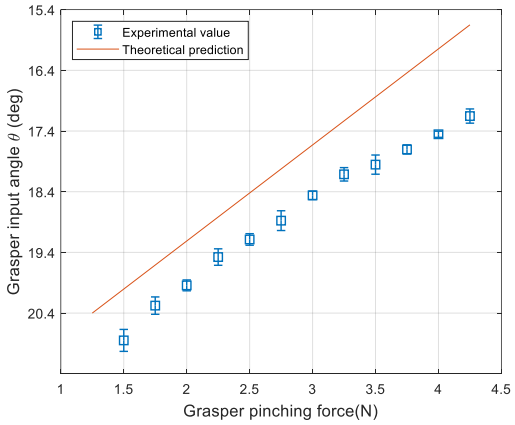

FIGURE 7: GRASPER ANGULAR POSITION VS GRASPER PINCHING FORCE

2.7 Grasper integration

The prototype grasper is integrated into a custom-built 6 DoF master arm, as shown in Figure 8. The grasper assembly is connected to the gimbal of the master arm, as shown. The Velcro straps of the grasper loop around the fingers and provide slip-free holding of the grasper. The grasper has adequate out of plane stiffness enabling the entire master arm to be moved within its workspace in all possible positions and orientations and functions well for its intended use [15].

3. DISCUSSION

The grasper could be statically balanced. But based on our discussion with robotic surgeons, and the design methodology followed by state-of-the-art devices, it is beneficial to have a lightly loaded return spring for the master arm grasper. Hence, there is no need for static balancing of the mechanism.

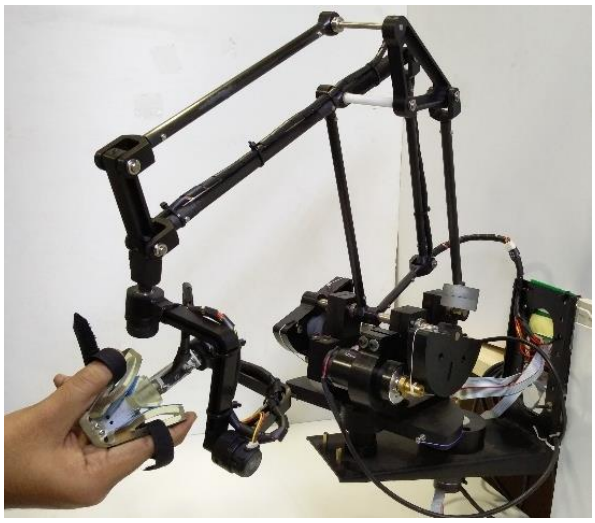

FIGURE 8: PROPOSED COMPLIANT GRASPER INTEGRATED TO A CUSTOM DESIGNED MASTER ARM [15]

Static balancing would cause the grasper not to return to its neutral position. Ergonomically it is easier for a surgeon to exert pinch force than pull force to open the grasper. The range of motion θ of the proposed grasper is taken as 4.5 degree to demonstrate the feasibility of working of the concept and can be increased further depending on the surgical application.

4. CONCLUSION

The design of a semi-compliant grasper for tele-robotic surgical applications has been presented. By using a small-length flexural pivot, a typical several-member design of a conventional grasper can be replaced by the proposed two-member compliant grasper. The mechanism has a spring-loaded follower which ensures contact between the follower and the grasper for any configuration, and thus prevents backlash. The motion of the grasper was smooth without any stiction during operation due to the presence of a plastic bearing liner at the joint interface. The proposed design has a linear relationship between the grasper input angle and follower displacement. Also, the mechanism exhibits a nearly linear relationship between the grasper pinching force input and the grasper deflection. The prototype demonstrates an avenue of using a flexure based compliant mechanism for grasper of a master arm in a surgical robot. Further works are in progress to optimize the dimensions of the grasper to improve the quality of force transfer. Investigations are also being carried out to increase the off-axis stiffness of the proposed grasper as the force required to move the entire master arm assembly is transmitted through the flexural pivot of the grasper.

REFERENCES

[1] Pugin, F., Bucher, P., and Morel, P., 2011. "History of robotic surgery: from AESOP® and ZEUS® to da Vinci®", *Journal of visceral surgery,* 148(5), pp.3-8. doi:10.1016/j.jviscsurg.2011.04.007.

[2] DiMaio, S., Hanuschik, M., and Kreaden, U., 2011. "The da Vinci surgical system," Surgical Robotics, Springer US. pp. 199-217. doi: 10.1007/978-1-4419-1126-1_9.

[3] 3D systems, Inc., 2020. "Phantom Premium", USA, accessed on November 1, 2020, https://www.3dsystems.com/haptics-devices/3d-systems-phantom-premium.

[4] Gerbi, C., R., Duval, E., F., Minami, D., Hager, B., Salisbury, J., K., Madhani, A., Stern, J., and Guthart, G., S., 2003. "Removable Infinite Roll Master Grip Handle and Touch Sensor for Robotic Surgery". U.S. Patent No. 6,587,750 B2.

[5] Mimic Technologies, Inc., 2020, "dV-Trainer®," Seattle, Washington, USA, accessed on November 1, 2020, http://www.mimicsimulation.com/dv-trainer.

[6] Miyazaki, R., Hirose, K., Ishikawa, Y., Kanno, T., and Kawashima, K., 2018, "A Master–Slave Integrated Surgical Robot With Active Motion Transformation Using Wrist Axis", *IEEE/ASME Transactions on Mechatronics*, *23*(3), pp. 1215-1225.

[7] Kota, S., Lu, K.-J., Kreiner, Z., Trease, B., Arenas, J., and Geiger, J., 2005. "Design and Application of Compliant Mechanisms for Surgical Tools". ASME *J. Biomech. Eng*., 127(6), pp. 981–989. doi:10.1115/1.2056561.

[8] Thomas, T. L., Kalpathy Venkiteswaran, V., Ananthasuresh, G. K., and Misra, S., 2021. "Surgical Applications of Compliant Mechanisms: A Review." ASME. *J. Mechanisms Robotics*, 13(2), pp. 020801. https://doi.org/10.1115/1.4049491.

[9] Salamon, B., A., Midha, A., 1998, "An Introduction to Mechanical Advantage in Compliant Mechanisms," ASME *J. Mech. Des*. 120(2), pp. 311-315. doi: 10.1115/1.2826974.

[10] Howell, L. L., 2001, Compliant Mechanisms, John Wiley & Sons, Inc., New York, USA, pp.135-141.

[11] Meriam, J., L., Kraige, L., G., 2012. Statics, John Wiley & Sons, Inc., Hoboken, New Jersey, pp. 337-339.

[12] Stratasys, Ltd., 2020. "PolyJet Materials Data Sheet," Stratasys, Eden Prairie, Minnesota, USA, accessed on November 1, 2020, https://www.stratasys.com/materials/search/veroclear.

[13] Igus, Inc., 2020. "iglide® tribo-tape A160," Igus, East Providence, Rhode Island, USA, accessed on November 1, 2020, https://www.igus.com/product/241.

[14] Howell, L. L., and Midha, A., 1994, "A Method for the Design of Compliant Mechanisms With Small-Length Flexural Pivots." ASME. *J. Mech. Des*. 116(1), pp. 280–290. doi: https://doi.org/10.1115/1.2919359.

[15] Chandrasekaran, K, Parameswaran, S., Annamraju S., Chandra, S., Manickam R., Thondiyath, A., 2021. "A Practical Approach to the Design and Development of Tele-operated Surgical Robots for Resource Constrained Environments – A Case Study", ASME *J. Med. Devices*, 15(1), pp.011105, doi: https://doi.org/10.1115/1.4049393.